

RESEARCH ARTICLE

10.1002/2016JD025160

Key Points:

- Aerosols from four agricultural areas are more ice active than desert dusts
- Soil dust particles are good candidates for ice nucleation in warm clouds
- The role of primary biological particles in soil dust agglomerates with regard to the observed ice nucleation properties remains unclear

Correspondence to:

I. Steinke,
isabelle.steinke@kit.edu

Citation:

Steinke, I., et al. (2016), Ice nucleation activity of agricultural soil dust aerosols from Mongolia, Argentina, and Germany, *J. Geophys. Res. Atmos.*, 121, 13,559–13,576, doi:10.1002/2016JD025160.

Received 12 MAY 2016

Accepted 18 OCT 2016

Accepted article online 20 OCT 2016

Published online 17 NOV 2016

Ice nucleation activity of agricultural soil dust aerosols from Mongolia, Argentina, and Germany

I. Steinke¹, R. Funk², J. Busse², A. Iturri³, S. Kirchen⁴, M. Leue², O. Möhler¹, T. Schwartz⁴, M. Schnaiter¹, B. Sierau⁵, E. Toprak¹, R. Ullrich¹, A. Ulrich⁶, C. Hoose¹, and T. Leisner^{1,7}

¹Institute of Meteorology and Climate Research, Karlsruhe Institute of Technology, Karlsruhe, Germany, ²Institute of Soil Landscape Research, Leibniz Centre for Agricultural Landscape Research, Müncheberg, Germany, ³Institute of Earth and Atmospheric Sciences, National University of La Pampa, Santa Rosa, Argentina, ⁴Institute of Functional Interfaces, Karlsruhe Institute of Technology, Karlsruhe, Germany, ⁵Institute for Atmospheric and Climate Science, ETH Zurich, Zurich, Switzerland, ⁶Institute of Landscape Biogeochemistry, Leibniz Centre for Agricultural Landscape Research, Müncheberg, Germany, ⁷Institute of Environmental Physics, Heidelberg University, Heidelberg, Germany

Abstract Soil dust particles emitted from agricultural areas contain considerable mass fractions of organic material. Also, soil dust particles may act as carriers for potentially ice-active biological particles. In this work, we present ice nucleation experiments conducted in the Aerosol Interaction and Dynamics in the Atmosphere (AIDA) cloud chamber. We investigated the ice nucleation efficiency of four types of soil dust from different regions of the world. The results are expressed as ice nucleation active surface site (INAS) densities and presented for the immersion freezing and the deposition nucleation mode. For immersion freezing occurring at 254 K, samples from Argentina, China, and Germany show ice nucleation efficiencies which are by a factor of 10 higher than desert dusts. On average, the difference in ice nucleation efficiencies between agricultural and desert dusts becomes significantly smaller at temperatures below 247 K. In the deposition mode the soil dusts showed higher ice nucleation activity than Arizona Test Dust over a temperature range between 232 and 248 K and humidities RH_{ice} up to 125%. INAS densities varied between 10⁹ and 10¹¹ m⁻² for these thermodynamic conditions. For one soil dust sample (Argentinian Soil), the effect of treatments with heat was investigated. Heat treatments (383 K) did not affect the ice nucleation efficiency observed at 249 K. This finding presumably excludes proteinaceous ice-nucleating entities as the only source of the increased ice nucleation efficiency.

1. Introduction

Aerosol particles influence cloud formation and properties. Thus, aerosols have a potentially large impact on the global climate and the hydrological cycle [Boucher et al., 2013]. One of the processes governing the interaction between aerosol particles and clouds is the initiation of droplet freezing in mixed-phase clouds at temperatures above 235 K [Pruppacher and Klett, 1997]. Such heterogeneous freezing processes require solid aerosol particles, so-called ice-nucleating particles (INPs), which facilitate the ice nucleation process. Below 235 K, only pure ice clouds, so-called cirrus clouds, exist which are formed either by heterogeneous ice formation processes involving INPs or by the homogeneous freezing of solution droplets [Vali et al., 2015].

Several ice nucleation modes have been hypothesized, namely, immersion/condensation freezing, deposition nucleation, and contact freezing [Vali et al., 2015]. Immersion freezing is initiated by aerosol particles within liquid cloud droplets, whereas condensation freezing occurs instantaneously within a thin layer of condensed water on the aerosol particle. Below ambient water saturation, pore condensation nucleation might occur in voids and cavities [Marcolli, 2014]. Water vapor directly being converted into ice at the surface of an aerosol particle is termed deposition nucleation. Contact freezing occurs when dry interstitial aerosol particles collide with supercooled cloud droplets and initiate freezing upon collision.

Only a minor fraction of all atmospheric aerosol particles acts as INPs in mixed-phase clouds [DeMott et al., 2010], and little is known about their surface properties and chemical composition. Nevertheless, several atmospheric particle species have been identified as potential INPs, ranging from biological particles such as bacteria, pollen, or fungi to mineral dust particles emitted from desert areas in North Africa and Asia [Hoose and Möhler, 2012; Murray et al., 2012]. Laboratory measurements (see references in Hoose and

Möhler [2012] and Murray *et al.* [2012]) and field studies [e.g., DeMott *et al.*, 2003; Pratt *et al.*, 2009; Prenni *et al.*, 2009; Cziczo *et al.*, 2013] showed that different particle species initiate the formation of cloud ice crystals preferentially at different temperature and humidity conditions, with biological particles often being ice-active at very high temperatures and mineral dust particles typically becoming active at temperatures below 253 K [Prenni *et al.*, 2009; Murray *et al.*, 2012]. In field studies it was observed that very ice-active biological particles in clouds may be cotransported with mineral dust particles [Pratt *et al.*, 2009; Hallar *et al.*, 2011; Creamean *et al.*, 2013]. These biological particles may cause freezing just below 273 K even in primarily dust-dominated clouds. A recent study confirmed that ice-nucleating proteins from soil fungi can adsorb to clay surfaces without compromising their ice nucleation efficiency [O'Sullivan *et al.*, 2016].

Agricultural areas in arid regions particularly contribute to dust plumes enriched in biological material. Even though atmospheric dust concentrations are largely dominated by emissions from desert areas, widespread intensification of land use has led to increasing emissions from agricultural areas [Ginoux *et al.*, 2012]. However, estimates regarding the contribution of agricultural areas to the global dust burden are not very well confined and range from less than 10% [Tegen *et al.*, 2004] to 20–50% [Funk and Reuter, 2006; Forster *et al.*, 2007; Ginoux *et al.*, 2012]. Nevertheless, due to the high mass fraction of presumably ice-active biological material accompanying agricultural soil dusts, even a minor contribution of soil dust sources to the total atmospheric dust burden may have a significant impact on the abundance of atmospheric particles nucleating ice in mixed-phase clouds [Conen *et al.*, 2011; O'Sullivan *et al.*, 2014]. In addition, atmospherically transported agricultural soil dust particles carry not only primary biological particles but also organic matter (OM) in various forms, such as free organic matter (e.g., leaf debris), organo-mineral complexes, and secondary organic compounds [Ellerbrock *et al.*, 2005; Kögel-Knabner *et al.*, 2008; Conen *et al.*, 2011; O'Sullivan *et al.*, 2014; Conen *et al.*, 2016].

Several laboratory studies have confirmed that soil dusts may include much more efficient INPs than desert dusts and clay minerals [Isono and Ikebe, 1960; Fornea *et al.*, 2009; Conen *et al.*, 2011; O'Sullivan *et al.*, 2014; Tobo *et al.*, 2014]. Therefore, soil dusts may initiate the formation of ice in droplet and mixed-phase clouds. Primary biological particles have been suspected to cause the enhanced ice nucleation capabilities of these soil particles [Schnell and Vali, 1972; Conen *et al.*, 2011; O'Sullivan *et al.*, 2014]. However, the ice nucleation active components of soil dusts have not been identified directly, leaving the role of soil organic matter (SOM) unclear [Isono and Ikebe, 1960; Fornea *et al.*, 2009; Conen *et al.*, 2011; O'Sullivan *et al.*, 2014].

The main focus of this work is the detailed investigation of the ice nucleation properties of four agricultural soil dust samples which was performed at the AIDA (Aerosol Interaction and Dynamics in the Atmosphere) cloud chamber. Additionally, the soil dust samples were characterized with respect to SOM composition, since organic components were suspected to contribute significantly to the observed ice nucleation efficiencies. The chemical composition and the properties of the OM were investigated by mass spectrometry, UV light-induced fluorescence, and infrared spectroscopy. Microbial colonization of soil dust was studied by cultivation of microorganisms and culture-independent estimation of the microbial abundance.

The number of biologically active particles was inferred from single particle mass spectrometry and fluorescence measurements. Additionally, DNA analyses provided information regarding the number of species and indications whether fungi or bacteria were more ubiquitous. The cultivation of filter samples with soil dust particles provided information on the viability of soil organisms. Since soil dust particles carry not only primary microorganism but also OM in various forms (e.g., organo-mineral complexes and coatings), we also investigated the chemical composition of SOM with Fourier transform infrared (FTIR) measurements.

All these methods are described in section 2. The results from the ice nucleation studies are presented in section 3 alongside with the chemical and microbiological analyses. Additionally, the ice nucleation efficiencies observed for the soil dusts were compared to results for desert dusts which are ubiquitous in the atmosphere but contain far less OM.

2. Methods

2.1. Sample Collection and Preparation

The soil samples investigated in this study are from four different regions of the world where land use changes have increased the problem of dust emissions [Tegen and Fung, 1995]. The samples were collected

Table 1. Overview of Soil Samples Used for Ice Nucleation Experiments

	Germany Brandenburg (GS)	Germany Baden-Württemberg (KS)	Argentina La Pampa (AS)	China Inner Mongolia (MS)
Geological origin	Fluvial deposits	Fluvial deposits	Aeolian deposits	Aeolian deposits
Land use	Arable land	Arable land	Arable land	Pasture
Soil texture	Sand/loamy sand	na	Sandy loam	Loam

in Southern Germany near Karlsruhe (sample name: KS), Northern Germany (GS), Mongolia (MS), and Argentina (AS). An overview of the samples is shown in Table 1.

The Chinese and Argentinian samples are from temperate grasslands (Xilingele steppe, Pampa), which are characterized by their vulnerability to wind erosion and large mass fractions of organic compounds [Shinoda *et al.*, 2011]. The conversion of former pastures into arable land to grow corn or soybeans has caused huge sand and dust storms in Argentina, blowing soil material into the Atlantic Ocean. Dust particles of the Province Buenos Aires could even be detected in ice probes of East Antarctica [Gaiero *et al.*, 2004]. In China, overgrazing has increased wind erosion of steppe soils [Yan *et al.*, 2005]. The sample from Northern Germany represents a typical sandy soil which is also prone to wind erosion processes [Funk *et al.*, 2004]. A further dust emission process in highly technologized agriculture is tillage, which affects all soils and amounts to the same magnitude as wind erosion. The sample from Southern Germany can be seen as an example for this releasing process.

All samples are taken from the topsoil (A horizon), in which decomposed OM is mixed with mineral components. It is also the zone with the highest microbial activity. The soil samples were air dried and stored in plastic bags. The samples were sieved to the particle fraction with diameters smaller than 63 μm .

At the same site where the AS sample was collected from the soil matrix, an additional sample was derived from dust that was trapped in 3.3 m height during a dust storm (AS_wind). This sample was not sieved.

A part of the AS sample (from the soil matrix) was exposed to heat (AS_heat: 383 K, 1 h). The treatment was intended to deteriorate proteinaceous structures such as the ice-active proteins associated with bacteria or fungi [Szymer and Zawadzki, 1997].

2.2. SEM Images of Single Particles

Images of single and agglomerated dust particles were gained from SEM (scanning electron microscope) analyses. Small amounts of dust from the bulk samples were placed on stubs, sputtered with gold-palladium, and investigated with a SEM (JEOL JSM6060 LV on SEI-mode).

2.3. Mass Fraction of Soil Organic Carbon

The mass fraction of soil organic carbon (SOC) was determined in a separate step (German Industry Standard ISO 10694, 1996). Organic and inorganic carbon compounds were analyzed with a LECO RC-612 multiphase carbon analyzer, which is able to differentiate between active, stable, and inorganic compounds of carbon by oxidation at different temperatures (300–350°C, 420–550°C, and > 1000°C) and relies on nondisperse infrared detection of CO₂ during dry combustion.

2.4. Analysis of OM Composition

In addition to quantifying the total SOM content, several methods were employed to better characterize the composition of OM for three samples, namely, MS, GS, and AS. The KS sample was only investigated with mass spectrometry due to the limited sample amount. SOM was intensively investigated in this study because its components were suspected to be the key factor for defining the ice nucleation properties of agricultural soil dusts.

2.4.1. Fourier Transform Infrared Spectroscopy

FTIR spectroscopy was employed to draw qualitative comparisons regarding the clay mineral content as well as the hydrophobicity of OM. For the FTIR measurements, 1 mg of each dust sample was mixed with 99 mg of potassium bromide (Merck, Darmstadt) and finely ground in an agate mortar. The mixtures were dried over

silica gel, and FTIR spectra were measured by using a FTS 135 spectrometer (BIO-RAD, Massachusetts, USA) at a resolution of $\Delta\tilde{\nu} = 1 \text{ cm}^{-1}$ in transmittance mode.

In the FTIR spectra, the signal intensities of absorption bands specific to OM were analyzed. The height values of C-H stretch vibrations of alkyl groups at $\tilde{\nu} = 2969 \text{ cm}^{-1}$, $\tilde{\nu} = 2928 \text{ cm}^{-1}$ (asymmetric stretching), and $\tilde{\nu} = 2859 \text{ cm}^{-1}$ (symmetric stretching) were measured as the vertical distance from a local "baseline" plotted between tangential points, added, and denoted as C-H bands [Ellerbrock *et al.*, 2005]. The absorption intensities of C=O double bonds were measured at $\tilde{\nu} = 1710 \text{ cm}^{-1}$ (ketones, carboxylic acids, or amides) [MacCarthy and Rice, 1985; Celi *et al.*, 1997] and at $\tilde{\nu} = 1627 \text{ cm}^{-1}$ and $\tilde{\nu} = 1611 \text{ cm}^{-1}$ (carboxylate anions and aromatic groups) [Gottwald and Wachter, 1997]. The C-H bands can be characterized as hydrophobic [Capriel *et al.*, 1995], and the C=O bands show hydrophilic behavior [Morrison and Boyd, 1986]. The ratio between C-H bands and C=O bands [Ellerbrock *et al.*, 2005] was used to characterize the potential wettability of the dust samples.

Clay-specific absorption was analyzed by measuring the absorption bands of O-H stretch vibrations of hydroxyl groups at $\tilde{\nu} = 3619 \text{ cm}^{-1}$ and of the Si-O-Al stretching at $\tilde{\nu} = 690 \text{ cm}^{-1}$ [Van der Marel and Beutelspacher, 1976; Madejova and Komadel, 2001].

2.4.2. Wideband Integrated Bioaerosol Sensor

During this study, the Wideband Integrated Bioaerosol Sensor (WIBS4—prototype designed and manufactured by the University of Hertfordshire) was used to investigate the occurrence of protein structures and the metabolic activity of organisms attached to soil particles, by sampling single particle fluorescence data for the different soil dust samples [Kaye *et al.*, 2005; Foot *et al.*, 2008; Toprak and Schnaiter, 2013]. WIBS4 has two filtered xenon lamps which excite tryptophan (280 nm) and nicotinamide adenine dinucleotide (NADH, 370 nm), respectively. NADH can be taken as indication for metabolic activity, whereas tryptophan is a part of protein structures but not necessarily associated with metabolic activity. Single particles are illuminated with UV light, and the resulting intrinsic fluorescence emitted by the particles is recorded in three fluorescence detection bands. These fluorescence detection bands are FL1: 310–400 nm (following the 280 nm excitation), FL2: 420–650 nm (following the 280 nm excitation), and FL3: 420–650 nm (following the 370 nm excitation). These ultraviolet light-induced fluorescence signals are used for the discrimination of biological from nonbiological particles.

Note that some mineral dusts such as Arizona Test Dust (ATD) fluoresce weakly between 300 nm and 420 nm after excitation with UV light [Pöhlker *et al.*, 2011]. Therefore, the background fluorescence caused by the mineral components of the soil dust particles was roughly estimated by investigating the fluorescence signals observed for ATD. The measurements were performed under controlled laboratory conditions in the aerosol preparation chamber next to the AIDA cloud chamber.

2.4.3. Mass Spectrometer

An aerosol time-of-flight mass spectrometer (ATOFMS, TSI Mode9I 3800, TSI Inc., St. Paul, MN, USA) was used to obtain information on the presence of biological material, internally or externally mixed with the dust aerosol. The ATOFMS [Gard *et al.*, 1997] determines the aerodynamic size and chemical composition of single particles in near real time. It uses an aerodynamic sizing technique to measure particle size and time-of-flight mass spectrometry to determine the chemical composition of particles. Particles in the size range of approximately 200 nm to 3 μm are drawn into the instrument from ambient air, sized, and due to the bipolar design of the mass spectrometer positive and negative ion spectra are acquired from each individual particle simultaneously. The ATOFMS deploys a 266 nm Nd:YAG laser desorption/ionization technique that allows the analysis of refractory material such as elemental carbon and mineral dust constituents.

For the identification of biological material, tracer ions like calcium, sodium, potassium, organic fragments, nitrate (a combination of both is often reflected in peaks at $^{26}\text{CN}^-$ and $^{42}\text{CNO}^-$), and phosphate can be used. However, as many of these elements are also present in mineral dusts [Gallavardin *et al.*, 2008] a clear identification of biological material in soil dust is highly challenging using this technique [Pratt *et al.*, 2009; Pratt and Prather, 2010; Cahill *et al.*, 2012; Cziczko *et al.*, 2013]. In this study, we used a rather simple screening for potentially biological material by querying the obtained single particle mass spectra of each soil sample (a) for the biomarkers $^{26}\text{CN}^-$, $^{42}\text{CNO}^-$, and $^{79}\text{PO}_3^-$ in absence of the dust markers aluminum $^{43}\text{AlO}^-$ and silicon $^{76}\text{SiO}_3^-$ (indication for externally mixed particles) and (b) for the biomarkers in the presence of the dust markers

(indication for internally mixed particles) using the TSI software MS-Analyze. The results presented depict the percentage of particles that contained the above mentioned combination of tracers.

As already noted, the identification of biological material in atmospheric aerosol particles using this method is difficult due to the potential presence of the listed biomarkers in nonbiological particles. This problem especially affects the ATOFMS analysis of soil dust since an overlap in ion traces resulting from dust and biological material is given. Also, ATOFMS reference spectra from soil dusts are limited. Therefore, the mass spectrometric results presented herein have to be interpreted with caution. A more detailed investigation of additional soil dust samples and different analytical approaches will be subject of a separate manuscript in preparation.

2.5. Characterization of Microbial Colonization

2.5.1. Analysis of Culturable Heterotrophic Bacteria

Qualitative comparisons regarding the numbers of viable microorganisms (e.g., bacteria) can be drawn from samples cultivated on R2A agar. From the AIDA cloud chamber, filter samples were drawn for approximately 20 min with a sample flow of 5 L/min (measured at standard conditions). For the experiments included in this study, the aerosol concentrations during sampling did not vary by more than a factor of 2 which makes the number of observed colonies approximately comparable. The filters (Whatman Nuclepore, 0.2 μm pore size, filter 111106) were then placed on standard R2A agar media and incubated for 5 days at 296 K. The filter housings were autoclaved prior to being connected to the AIDA cloud chamber. Also, the equipment used during the handling of the filter samples was disinfected. Blank filter samples showed no signs of bacterial contamination. Note that only one filter sample was drawn during each AIDA expansion run, and thus, these results can only be taken as a rough estimate for the number of colony-forming microbes in the aerosol.

2.5.2. DNA Extraction and Analysis of the Abundance of Bacteria, Fungi, Actinobacteria, and *Pseudomonas* as Determined by Real-Time PCR

The number fraction of fungi and bacteria was investigated in more detail by using DNA analyses. Within bacteria, we studied the abundance of the phylum Actinobacteria as well as the important group of *Pseudomonads* which are potentially active in ice nucleation. However, it should be noted that this method was not used to directly identify and analyze ice-nucleating organisms. The advantage of a DNA-based real-time polymerase chain reaction (PCR) approach is the feasibility of a culture-independent quantification of the microbial groups with viable but not culturable, dormant and dead cells as well as free DNA being detected [Willerslev *et al.*, 2004].

Total DNA was extracted from three aliquots (0.1 g) of the dust samples using the NucleoSpin Soil Kit (Macherey-Nagel, Germany) according to the manufacturer's instructions. Mechanical cells lysis was achieved by applying the FastPrep-24 Instrument (40 s at 6.0 ms^{-1}) (MP Biomedicals, Germany). Diluted DNA samples were subjected to real-time PCR using the QuantiTect SYBR Green PCR kit (Qiagen, Germany). Quantification of the 16S rRNA gene for bacteria, actinobacteria, and the genus *Pseudomonas* was performed as described by Becker *et al.* [2014].

The abundance of fungi was estimated by quantifying the ITS rRNA region [Fierer *et al.*, 2005]. Two independent PCR reactions were performed using an ABI Prism 7500 Fast Thermal Cycler (Life Technologies, Germany). Inhibitory effects of the DNA extracted from dust samples on PCR performance were tested by quantification of serial dilutions. The copy number of the fungal ITS rRNA region was calibrated with known amounts of pure-culture fungal spores of *Fusarium graminearum*.

2.6. AIDA Cloud Chamber Experiments

The ice nucleation properties of four soil dust samples (see Table 1) were investigated at the AIDA cloud chamber facility (Karlsruhe Institute of Technology, Germany).

The cloud chamber is generally used to simulate atmospheric trajectories of ascending air parcels by expanding moist air within the cloud chamber vessel, starting from a predefined temperature near the expected freezing conditions and ambient pressure. Mixed-phase and cirrus cloud conditions can be simulated alike, and the ice nucleation properties of aerosol particles are investigated under atmospherically relevant conditions.

For each experimental run, temperature and relative humidity over water and over ice are measured simultaneously together with the concentrations of droplets and ice crystals.

The gas temperature within the AIDA cloud chamber vessel is measured by several well-calibrated sensors with a measurement uncertainty $\Delta T = \pm 0.1$ K. The variability of individual gas temperature sensors with respect to their overall mean value is typically less than $\Delta T = \pm 0.3$ K [Möhler *et al.*, 2006]. The temperature at the chamber walls is also measured during expansion experiments but generally does not change much from the initial temperature at the beginning of an expansion run. The relative humidity values are derived from tunable diode laser absorption measurements which deliver the water vapor concentration within the AIDA cloud chamber. The absolute water vapor concentration values are then converted into relative humidity values by normalizing with the saturation vapor pressure over ice and over water, respectively, as parameterized by Murphy and Koop [2005]. The relative humidity values are determined within $\Delta RH = \pm 5\%$ [Fahey *et al.*, 2014].

The droplet and ice crystal concentrations are derived from measurements with two optical particles counters (welas, Palas GmbH) which in combination cover a size range from 0.7 to 240 μm (referring to liquid water droplets) [Wagner and Möhler, 2013]. Prior to injection into the AIDA cloud chamber, the dry dust samples are dispersed by a rotating brush generator (RBG1000, Palas) which is used in combination with cyclone impactor stages eliminating particles larger than 5 μm . The aerosol size distribution of particles in the AIDA chamber is derived from APS (Aerodynamic Particle Sizer, Model 3321, TSI) and SMPS (Scanning Mobility Particle Sizer, Model 3071, TSI) measurements. The aerosol number size distribution is then used to calculate the aerosol surface area concentration for each experiment by using the volume-equivalent sphere diameters [Möhler *et al.*, 2006]. All experiments which were conducted at the AIDA cloud chamber to investigate the ice nucleation properties of the four soil samples are listed in Table 2. The experiments are sorted regarding the ice nucleation mode that was observed with immersion freezing occurring at temperatures above 245 K and deposition nucleation at lower temperatures and below saturation with respect to water. Table 2 also lists the temperature at the beginning of each individual expansion experiments and the aerosol size distribution parameters.

For each experimental run, the ice nucleation efficiency is expressed as the ice nucleation active surface site (INAS) density n_s [m^{-2}] which is given by

$$n_s = n_{\text{ice}}/A_{\text{aer}} \quad (1)$$

where $n_{\text{ice}}[\text{cm}^{-3}]$ is the observed ice crystal concentration and $A_{\text{aer}}[\mu\text{m}^2\text{cm}^{-3}]$ the aerosol surface area concentration [Connolly *et al.*, 2009; Hoose and Möhler, 2012; Niemand *et al.*, 2012]. Note that for analyzing the immersion freezing experiments, the aerosol surface area concentration is typically scaled according to the ratio of the droplet and aerosol number concentrations in order to account for the fact that particles will only participate in immersion freezing after having been activated to droplets. We assume that all particles have been activated to droplets, whereas during the initial phase of an expansion experiment this might lead to an overestimation of the aerosol surface area. The measurement uncertainty of the INAS density is determined by the measurement uncertainty of the ice crystal concentration ($\Delta n_{\text{ice}}/n_{\text{ice}} \approx 25\%$) and the aerosol surface area ($\Delta A_{\text{aer}}/A_{\text{aer}} \approx 25\%$), yielding $\Delta n_s/n_s \approx 35\%$.

The INAS density values describe the average ice nucleation efficiency of an aerosol population as a function of temperature ($T[\text{K}]$) for immersion freezing and, additionally, of the saturation ratio with respect to ice (S_{ice}) for deposition nucleation. Note that this approach neglects a possible time scale dependence of the ice nucleation process.

3. Results

3.1. Characteristics of Soil Dust Samples

3.1.1. Microscope Images of Soil Dust Particles From the Bulk Samples and Surface Area Distribution Within the AIDA Cloud Chamber

Figure 1 depicts SEM images of two different types of dust particles from the MS sample (Figures 1a and 1b) and from ATD (Figures 1c and 1d). SEM images were taken for bulk samples of both dust types. Note that ATD ($d = 0\text{--}3$ μm) consists of processed desert dust which was milled, sieved, and washed.

The MS sample is characterized by a larger particle heterogeneity than ATD. Although ATD particles tend to agglomerate to entities larger than 20 μm , single particles are much smaller than found in the Mongolian sample where smaller particles typically adhere to larger particles.

Table 2. Overview of AIDA Cloud Chamber Experiments With Karlsruhe Soil (KS), German Soil (GS), Mongolian Soil (MS), and Argentinian Soil (AS)

Experiment	Aerosol	Initial Temperature (K)	Aerosol Concentration (cm^{-3})	Aerosol Surface Area Concentration ($\mu\text{m}^2 \text{cm}^{-3}$)	Median Diameter (μm)	Ice Nucleation Mode
INUIT08_04	GS	266	220	423	1.25	Immersion freezing
IN16_02	KS	264	230	283	0.75	Immersion freezing
IN16_09	KS	264	232	262	0.78	Immersion freezing
IN15_56	KS	262	268	719	1.37	Immersion freezing
INUIT08_03	GS	262	210	372	1.28	Immersion freezing
INUIT08_05	MS	262	211	387	1.43	Immersion freezing
INUIT08_02	MS	261	96	221	1.50	Immersion freezing
IN19_07	AS	259	138	126	0.80	Immersion freezing
INUIT08_01	MS	258	193	203	1.00	Immersion freezing
IN19_05	MS	258	95	68	0.74	Immersion freezing
IN19_06	GS	258	124	152	0.84	Immersion freezing
IN19_43	AS	254	165	145	0.75	Immersion freezing
IN19_44	AS_heat	254	132	167	0.84	Immersion freezing
IN19_46	GS	255	167	170	0.71	Immersion freezing
INUIT04_40	AS	249	260	192	0.55	Deposition nucleation
IN19_09	AS	248	144	116	0.69	Deposition nucleation
INUIT04_32	MS	248	133	355	1.40	Deposition nucleation
IN19_31	AS_heat	248	224	159	0.69	Deposition nucleation
IN19_33	GS	248	194	88	0.54	Deposition nucleation
IN19_11	MS	247	124	107	0.67	Deposition nucleation
IN19_18	AS_wind	247	121	156	0.86	Deposition nucleation
IN15_51	KS	242	339	354	0.73	Deposition nucleation
INUIT04_46	MS	238	112	57	0.51	Deposition nucleation
INUIT04_48	AS	238	269	198	0.56	Deposition nucleation
IN15_50	KS	233	295	456	1.24	Deposition nucleation

The observed particle morphologies suggest that the soil dust from Mongolia contains plant debris and mineralized plant cell structures (phytoliths) in addition to mineral particles. In contrast, ATD almost exclusively consists of mineral particles. For the soil dust, particles of biological origin were often larger than $20 \mu\text{m}$. Similar phytolith structures and plant debris were found in all soil samples (not shown).

Figure 2 shows a surface area distribution of aerosol sampled from the AIDA cloud chamber. Particles larger than $5 \mu\text{m}$ are effectively eliminated by using cyclone impactors. Therefore, the aerosol size distribution of

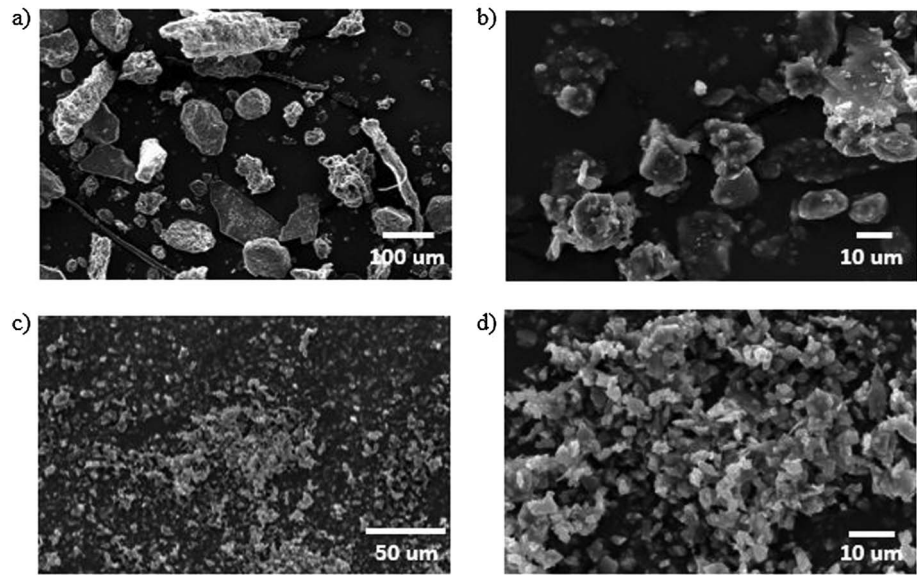


Figure 1. SEM images showing the morphology of (a, b) MS particles in comparison to (c, d) ATD.

particles within the AIDA chamber can be considered to be representative for long-range transported dust plumes in the middle and upper troposphere.

3.1.2. FTIR Measurements

The FTIR measurements deliver insights both into the organic and mineral compounds of soil dust samples. Three soil samples (GS, AS, and MS) were analyzed and compared with ATD.

Table 3 represents the absorption intensities measured with FTIR spectroscopy (relative to an individual baseline). Additionally, the mass fractions of total SOC are given.

The clay-specific absorption intensities of the soil dusts as inferred from the Si-O-Al band at $\tilde{\nu} = 690 \text{ cm}^{-1}$ are by a factor of 2 lower for the MS and AS samples compared to ATD and by a factor of 4 for the GS sample compared to ATD as well. This result confirms that agricultural soil dust particles contain significant amounts

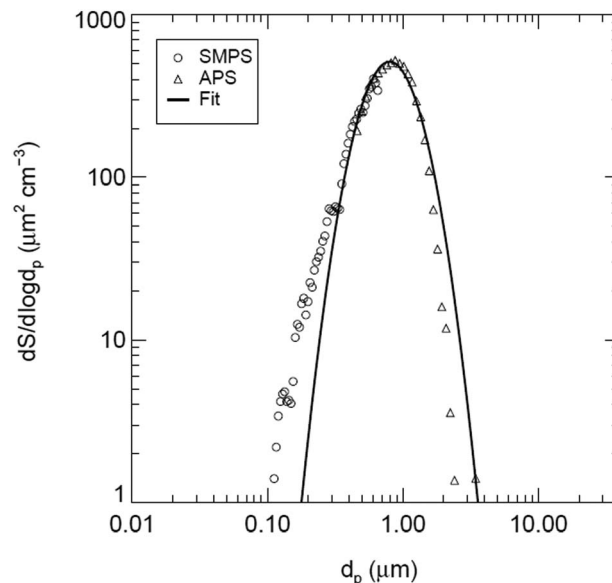


Figure 2. Aerosol surface area distribution for soil dust particles sampled from the AIDA cloud chamber prior to an experimental run (sample: KS).

Table 3. Absorption Band Intensities of Clay Mineral-Specific OH Groups, Aliphatic C-H Groups, and Carbonylic/Carboxylic C=O Groups, As Well As Water Repellency (C-H/C=O Ratio) of OM^a

Measured Variable		Germany Brandenburg (GS)	Argentina La Pampa (AS)	China Inner Mongolia (MS)	ATD
Mineral components	Clay mineral-specific absorption (a.u.)	0.052	0.081	0.095	0.190
Organic matter	Total organic carbon (Mass %)	2.89	1.45	2.49	n.a.
	Summed C-H groups of OM (a.u.)	0.0210 ± 0.0020	0.0060 ± 0.0001	0.0140 ± 0.0003	0.0080 ± 0.0010
	Summed C=O groups of OM (a.u.)	0.22 ± 0.07	0.19 ± 0.01	0.23 ± 0.02	0.23 ± 0.01
	C-H/C=O ratio	0.095 ± 0.025	0.033 ± 0.002	0.062 ± 0.006	0.038 ± 0.002

^aDerived from FTIR spectroscopy measurements of GS, AS, and MS soil dust samples compared to the properties of ATD.

of nonmineral components in contrast to ATD particles containing more than 40% clay minerals [Broadley *et al.*, 2012].

The absorption signal intensities of the aliphatic C-H functional groups (representing hydrophobic OM components) are lowest for ATD and the AS sample (Table 3). Even though the ATD sample is expected to hardly contain any OM, the FTIR spectra of ATD clearly showed small C-H and C=O absorption bands.

The dusts from Northern Germany and Mongolia were characterized by C-H absorption signals which were higher by a factor of 2–3 compared to the AS sample. This observation can be taken as an indication for the higher OM content of these two samples. Further confirmation of this trend is provided by measurements of the total organic carbon content, which is lowest for the AS sample. The absorption observed at the C=O bands (related to the fraction of hydrophilic OM) was similar among all dusts. The GS sample had the highest C-H/C=O ratio which suggests the lowest potential wettability of the OM among the measured samples.

3.1.3. WIBS4 Measurements

In this study, the fluorescence of ATD particles was used as a proxy for the cross sensitivity of the WIBS instrument to signals caused by nonbiological components of the soil dust samples. Approximately 1% of all ATD particles showed fluorescence despite presumably negligible contributions by biological particles adhering to the dust. Therefore, 1% of the total number of particles was attributed to this cross sensitivity and consequently subtracted from the number of fluorescing particles (N_{F1} , N_{F2} , and N_{F3}). Subscripts refer to the three fluorescence detection channels with FL1: 310–400 nm (following the 280 nm excitation), FL2: 420–650 nm (following the 280 nm excitation), and FL3: 420–650 nm (following the 370 nm excitation). It should be noted that this cross sensitivity is only a very rough estimate and needs to be verified in further studies.

After characterization of the cross sensitivity of the WIBS4 instrument, the fractions of particles with fluorescence signatures indicating the presence of primary biological particles were determined for three samples (AS, GS, and MS).

Table 4 shows particle fractions of fluorescing particles as detected by the three different WIBS4 channels. Note that the WIBS4 detects particles with optical sizes between 0.5 and 16 μm [Toprak and Schnaiter, 2013]. The fraction of particles containing tryptophan (N_{F1}/N_T) is highest for the sample from Mongolia (9%), whereas this fraction is similar for the GS sample ($\approx 3\%$) and the AS sample ($\approx 5\%$). The fraction of particles with metabolic activity (N_{F3}/N_T) is below the detection limits for GS and AS. Although further investigations should be conducted, the ratio N_{F3}/N_T for the MS sample indicates a higher number of viable organisms than for the other soil samples. Note that the fluorescence signals measured for the second channel (N_{F2}) indicate a similar trend as the fraction of particles containing tryptophan.

Table 4. Particle Fraction of Biologically Active Particles (%)^a

	N_{F1}/N_T	N_{F2}/N_T	N_{F3}/N_T
GS	3.0 ± 1.0	1.0 ± 1.0	-
AS	5.0 ± 1.0	2.0 ± 2.0	-
MS	9.0 ± 1.0	3.0 ± 1.0	1.0 ± 0.1
AS_heat	2.5 ± 0.3	-	-

^a N_{F1} and N_{F2} refer to the number of particles containing tryptophan, whereas N_{F3} denotes the number of particles containing NADH; N_T is the number of detected particles.

Table 5. Abundance of Microbial Groups as Determined by the Quantification of the 16S rRNA Gene as Well as the Fungal ITS Region^a

	Germany Brandenburg (GS)	Argentina La Pampa (AS)	China Inner Mongolia (MS)
Bacteria	$(1.2 \pm 0.3) \cdot 10^9$	$(1.4 \pm 0.2) \cdot 10^9$	$(2.4 \pm 0.2) \cdot 10^9$
Actinobacteria	$(8.2 \pm 1.5) \cdot 10^8$	$(9.1 \pm 1.0) \cdot 10^8$	$(2.3 \pm 0.2) \cdot 10^9$
<i>Pseudomonas</i>	$(2.9 \pm 0.9) \cdot 10^6$	$(1.5 \pm 0.6) \cdot 10^5$	$(2.1 \pm 1.6) \cdot 10^5$
Fungi	$(4.1 \pm 1.0) \cdot 10^7$	$(2.6 \pm 0.5) \cdot 10^6$	$(1.9 \pm 0.2) \cdot 10^6$

^aMean values and standard deviation are given (copy number of the 16S rRNA gene or number of fungal spores (g^{-1} soil dust)).

For the Argentinian Soil samples which were heated, the contribution by fluorescing biological particles was significantly reduced to less than half compared to the untreated samples. For the treated dust, reliable fluorescence signals could only be detected with the first channel (F1) of the WIBS4 instrument.

In conclusion, the WIBS4 measurements indicate that the MS sample contains significantly more surface protein structures than the two other samples. Additionally, the heat treatment led to a significant deterioration of these protein structures.

3.1.4. Mass Spectrometer

The percentage of particles (aerodynamic diameter $<3 \mu\text{m}$) with biological signatures was also determined from single particle mass spectrometry. The presence of biological particles was inferred from tracer ions ("biomarkers"). As a reference, ATD representing "pure" dust was investigated with a similar analytical approach. The mass spectral analysis of ATD particles revealed about 1% of particles with only biomarkers (externally mixed) and 32% with both biological and mineralogical signatures (internally mixed particles). The biomarkers indicate the presence of OM, not necessarily being restricted only to biological particles such as bacteria or fungi.

The soil samples contained at least 5% particles with only biomarkers and 24% internally mixed ones. In more detail, the GS and AS sample analysis revealed 12% resp. 5% in the first case, whereas the sample from Karlsruhe and the MS sample were characterized by similar fractions of particles containing organic markers (17%). Comparing the internally mixed fractions of the KS sample, MS, GS, and AS contained 67%, 45%, 32%, and 24%, respectively.

3.1.5. Quantification of Bacteria and Fungi in the Soil Dust Samples by PCR Analysis

The abundance of total bacteria ranged from $1 \cdot 10^9$ to $2 \cdot 10^9$ 16S rRNA gene copies per gram soil dust. The GS and AS samples contained slightly fewer bacterial cells than the MS sample (Table 5). A large fraction of the detected bacteria belonged to the phylum Actinobacteria (between 60 and 90%), whereas bacteria belonging to the genus *Pseudomonas* were much less abundant by several orders of magnitudes. Fungi were most abundant in the GS sample but were underrepresented compared to bacteria in all three samples based on the copy numbers of the ribosomal operons. None of the microbial groups were detected in ATD.

3.1.6. Abundance of Culturable Heterotrophic Bacteria

Figure 3 shows filter samples which were taken from the AIDA cloud chamber and then incubated on R2A agar.

MS (Figure 3a) particles contained least culturable cells. Only very few (~5) colonies grew after incubation. In contrast, the GS sample showed more than 100 (Figure 3b) and the Argentinian Soil sample even more than 250 colony-forming units with varying morphological properties (Figure 3c). The aerosol number concentrations within the AIDA cloud chamber were comparable during all three experiments. Thus, the number of microorganisms which favored the selected growth conditions was highest for the Argentinian Soil sample. The fraction of particles containing culturable bacteria was estimated from the number of colony-forming units (CFUs), the sampling time of roughly 20 min at a flow of 5 L/min, and the aerosol number concentration within the AIDA chamber. For all three samples, this fraction was below 1‰.

Treating the Argentinian Soil sample with heat resulted in a significant reduction in the number of microorganisms that are able to grow on R2A agar (Figure 3d). For the heat-treated dust sample only ~25 CFUs were found.

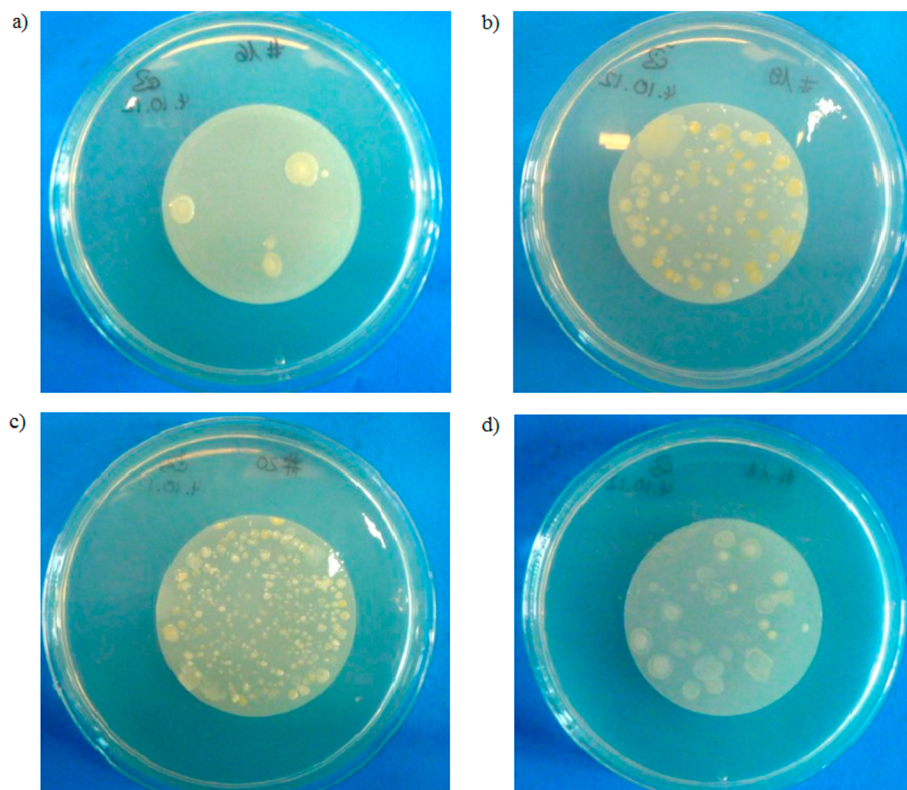


Figure 3. Filter samples with agricultural soil dust particles (extracted from the AIDA cloud chamber) after cultivation on R2A agar—number of colony-forming units clearly visible: (a) MS, (b) GS, (c) AS, and (d) AS (heat treated).

3.1.7. Summary

Table 6 provides a summary of all measurement results regarding the abundance of biologically active particles. The AS dust was identified as the sample with the lowest number of biologically active particles. Between GS and MS which were ranked similar, the sample from Mongolia most likely contained the highest number of biologically active particles. The number of culturable bacteria did not correlate with the total number of biologically active particles. The AS sample contained the highest number of culturable bacteria among the three samples.

3.2. Ice Nucleation Efficiency of Soil Dust Samples

The ice nucleation efficiencies of the four soil dust samples (see Table 1) were determined from AIDA cloud chamber experiments. Additionally, the impact of heat (383 K) on the ice nucleation efficiencies was

Table 6. Summary of Results for the Abundance of Biologically Active Particles: Abundance Indicated as Low (+) to High (+++)

	Germany Brandenburg (GS)	Argentina La Pampa (AS)	China Inner Mongolia (MS)	Measured Indicator
Total organic carbon	++	+	++	Mass fraction of total organic carbon
FTIR	++	+	++	(Hydrophobic) OM
WIBS4	+	+	++	Protein structures
ATOFMS	++	+	+++	Particles with biomarkers
PCR analysis				Number of cells and cell fragments
Bacteria	+	+	++	
Fungi	++	+	+	
Cultivation on R2A	++	+++	+	Number of viable cells

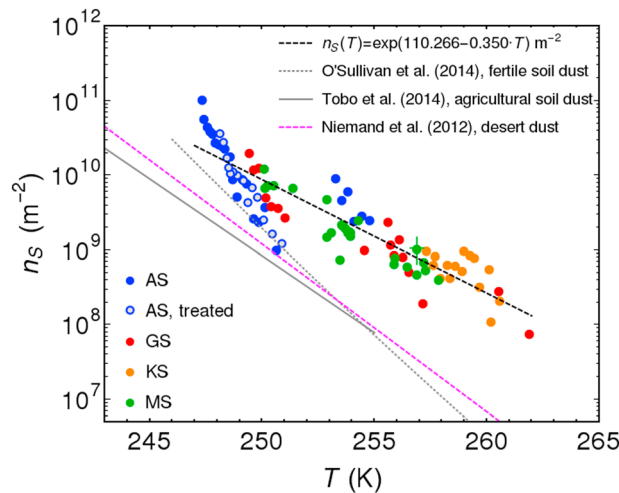


Figure 4. Results for immersion freezing initiated by agricultural soil dust particles—the ice nucleation efficiencies are expressed as INAS densities in relation to temperature T .

investigated for the Argentinian Soil dust sample. Ice nucleation was observed in the immersion freezing and the deposition nucleation mode.

Figure 4 shows the INAS densities for the four soil dust samples for immersion freezing. Additionally, the INAS density values observed for heat-treated Argentinian Soil dust are shown. The INAS density values are represented in relation to the temperature $T_{\text{gas}}[\text{K}]$ in the AIDA cloud chamber.

The ice nucleation properties were observed over a temperature range between 247 and 262 K. For the KS sample, only experimental runs at temperatures between 257

and 261 K were conducted. Especially, the experimental data for the AS sample demonstrate that ice nucleation properties of each agricultural soil dust in this study are variable within 1 order of magnitude.

Between 250 and 255 K, the INAS densities of AS, MS, and GS are remarkably similar. Based on this trend, an average INAS density of the four soil samples can be approximated by a temperature (T in [K])-dependent function which is given by

$$n_s(T) = \exp(110.266 - 0.350 \cdot T) \text{ [m}^{-2}\text{]} \quad (2)$$

for temperatures between 247 and 262 K.

For comparison, the average INAS density values for desert dusts [Niemand et al., 2012] and several other soil dusts [O'Sullivan et al., 2014; Tobo et al., 2014] are represented in Figure 4. The investigated soil dust samples are on average more ice active than desert dusts which are presumed to contain fewer primary biological particles, such as fungi, bacteria, and plant debris, and also less OM. Close to 246 K, however, the difference in the ice nucleation efficiencies between soil samples and desert dusts gradually becomes smaller. Therefore, the soil-specific components seem to be especially relevant for immersion freezing at higher temperatures. The heat treatment targeting biological ice nucleation components did not affect the ice nucleation properties of the AS sample in the temperature range between 247 and 251 K.

In comparison to the soil dusts that were investigated in the study by O'Sullivan et al. [2014], the samples investigated in this study were more ice active, especially at temperatures above 252 K. Tobo et al. [2014] observed ice nucleation efficiencies for agricultural dusts from two sites in Wyoming and found similar INAS densities as O'Sullivan et al. [2014] for their samples.

Ice nucleation was also investigated for deposition mode ice nucleation at temperatures below 248 K and subsaturation with respect to water (i.e., above saturation with respect to ice, $S_i > 1$).

Figure 5a shows the trajectories and single data points within the T - S_i space for which ice nucleation properties were measured. As for immersion freezing, INAS densities were derived for all four dust samples and the heat-treated AS sample. Additionally, the ice nucleation properties of wind-blown AS dust were investigated. All trajectories are located below water saturation which is indicated by a dashed black line.

In Figure 5b, the deposition nucleation mode efficiencies for all experiments conducted in this study are represented as a function of saturation with respect to ice (S_i). As deposition nucleation also depends on the ambient temperature, in Figure 5b the temperatures at the beginning of each experimental run are also indicated. For runs with starting temperatures between 243 and 248 K, lower INAS density values were observed than for experiments starting temperatures below 241 K, with INAS density values ranging between

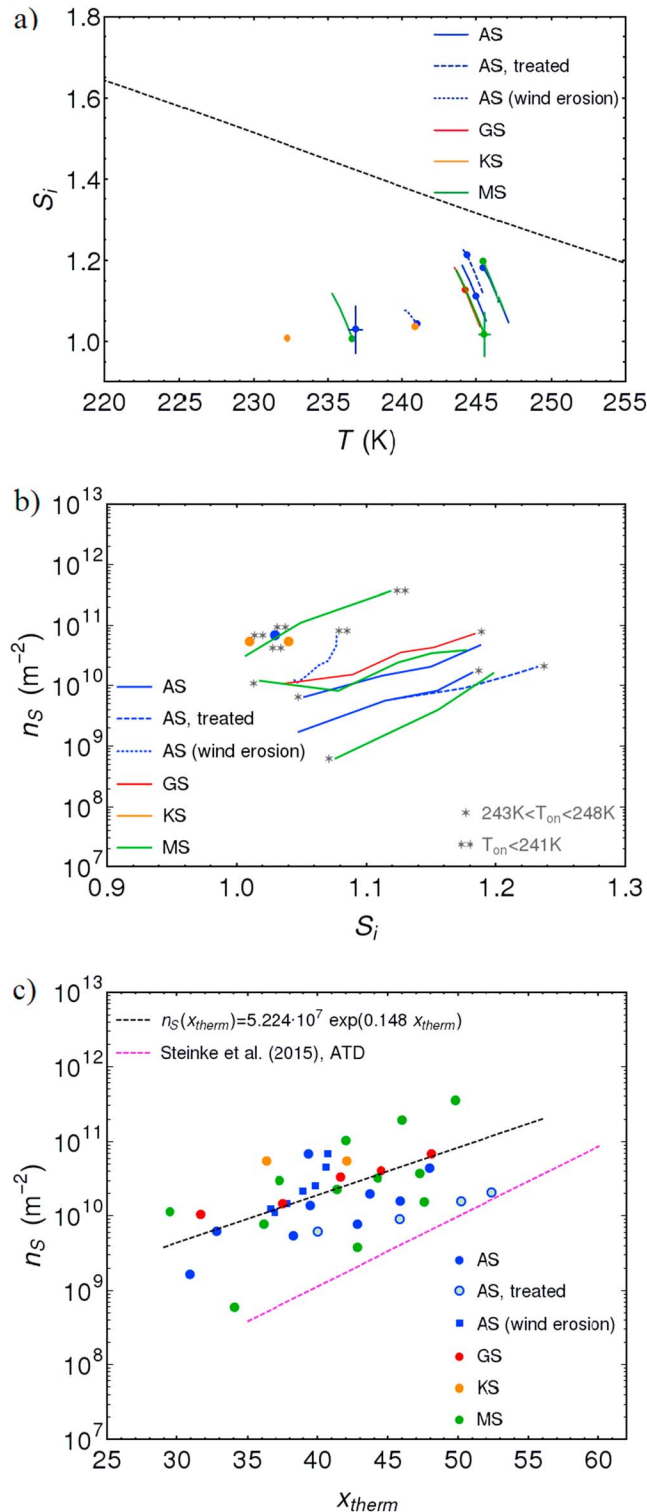


Figure 5. Results for deposition nucleation initiated by agricultural soil dust particles—trajectories of expansion runs shown in (a) and ice nucleation efficiencies expressed as INAS densities in relation to (b) S_{ice} and to the thermodynamic function (c) X_{therm} .

10^9 and $10^{11} m^{-2}$. Figure 5b shows that the INAS density values group according to the starting temperature. Within these temperature groups, the observed trend is similar as for immersion freezing: the INAS density values for GS, AS, and MS vary within 1 order of magnitude, with already considerable variability observed for each soil dust individually. Similarly as for immersion freezing caused by the AS sample, no impact of heat treatment can be inferred for deposition nucleation observed for this specific sample. The AS sample which was collected by trapping wind-blown dust activates within the range of relative humidities observed for the top soil sample.

In Figure 5c, INAS density values are related to a function of temperature (T) and the saturation ratio over ice (S_i) which are combined into the thermodynamic function X_{therm} with

$$X_{therm} = -(T - 273.15) + (S_i - 1) \times 100 \quad (3)$$

This function was introduced to represent the dependence of deposition nucleation on temperature and humidity. Equation (3) serves as a good approximation of the temperature and humidity dependence observed for high-temperature deposition nucleation, e.g., for ATD [Steinke et al., 2015]. With this composite representation stated in equation (3), INAS density values can be better compared among experiments with different starting temperatures. The X_{therm} formulation as a first-order approximation should be considered as a starting point for further developing parameterizations, analogously to the INAS density function for immersion freezing. A higher-order fit regarding

the temperature and humidity dependence may be more realistic but would require more data from different samples and in a wider range of temperature and relative humidity.

In addition to the INAS density values from Figure 5b, the ice nucleation efficiency observed for ATD is also depicted in Figure 5c [Steinke *et al.*, 2015]. ATD is only slightly more efficient than the soil dusts, considering the large variability of observed INAS density values.

As for the immersion freezing experiments, the INAS density for deposition nucleation initiated by soil dusts can be approximated by a function depending on the thermodynamic function x_{therm} with

$$n_s(x_{\text{therm}}) = 5.224 \times 10^7 \cdot \exp(0.148 \cdot x_{\text{therm}}) \quad [\text{m}^{-2}] \quad (4)$$

The relation stated in equation (4) is valid for temperatures between 233 and 246 K and relative humidity over ice varying between 100 and 125%. The measurement uncertainties are given by $\Delta T = \pm 0.3$ K, $\Delta \text{RH}_{\text{ice}}$ up to 5% (i.e., $\Delta x_{\text{therm}} \approx 5$), and $\Delta n_s/n_s \approx 35\%$ [Möhler *et al.*, 2008; Fahey *et al.*, 2014; Steinke *et al.*, 2015].

4. Discussion

For a temperature range between 233 and 262 K, the immersion and deposition mode ice nucleation efficiencies of the four soil dust samples investigated in this study were described by average ice-active surface site density relations (i.e., exponential functions).

The soil dust samples are more ice active than desert dusts in the immersion freezing mode at temperatures above 246 K. In the deposition nucleation mode, initial comparisons showed that agricultural soil dusts are slightly more ice active than ATD for temperatures between 233 and 246 K and humidities below $\text{RH}_{\text{ice}} = 125\%$.

In the following paragraphs, we will focus the discussion on immersion freezing studies with agricultural soil dusts. Our findings regarding the enhanced ice nucleation properties agree conceptually with a study by Conen *et al.* [2011] on the freezing properties of suspensions containing soil dusts from Western Mongolia, Southern Germany, Hungary, or Yakutia. These soil dust samples showed higher or at least similar mass-related site density values than montmorillonite for temperatures between 258 and 263 K.

In contrast to our results, three out of four soil dust samples investigated by O'Sullivan *et al.* [2014] showed INAS densities similar to desert dusts investigated by Niemand *et al.* [2012], even at temperatures above 255 K. Also, the study by Tobo *et al.* [2014] found INAS densities for two agricultural dust samples from Wyoming which are similar to desert dusts.

Note, however, that O'Sullivan *et al.* [2014] estimated the relevant aerosol surface area from diffraction measurements, whereas the parameterization describing the freezing efficiency of desert dusts [Niemand *et al.*, 2012] is based on APS and SMPS measurements. Tobo *et al.* [2014], in contrast, derived the aerosol surface area based on assuming spherical particles with a diameter of 600 nm. Systematic differences between the underlying aerosol surface areas may at least partially explain the lower INAS densities measured by O'Sullivan *et al.* [2014]. It should also be considered that two of the previously mentioned studies [Conen *et al.*, 2011; O'Sullivan *et al.*, 2014] use soil dust suspensions. A study comparing ice nucleation measurements of illite particles [Hiranuma *et al.*, 2015] revealed differences in observed ice nucleation efficiencies, depending on the experimental setup and also the particle preparation (i.e., dry dispersion compared to particle suspensions). Additionally, Conen *et al.* [2011] only present mass-related ice nucleation efficiencies instead of surface related values. Variations in the particle size distributions might therefore be reflected in an apparent change of the mass-related ice nucleation properties. Above all, without direct intercomparison studies investigating the ice nucleation properties of one soil sample, it is not possible to discriminate between setup-related and soil-specific variability.

The results of this study with soil particles showing enhanced ice nucleation properties at high temperatures also agree with other studies [Schnell and Vali, 1972; Vali, 2008; Fornea *et al.*, 2009]. These observations suggest that the increased ice nucleation efficiency observed for soil dusts may be caused by soil organisms such as bacteria or fungi [Christner *et al.*, 2008; Després *et al.*, 2012]. Interestingly, Tobo *et al.* [2014] did not find phosphorus markers in their samples which they attribute to the absence of microorganisms.

For our samples we found indications for microbiological activity (cf. Table 6). However, primary biological particles do not always seem to be the determining factor for soil dust ice nucleation, with no consistent

trend between microbiological activity and ice nucleation efficiency. Also, heat treatment intended to destroy ice-active proteins associated with biological particles did not affect the ice nucleation efficiency of the AS sample at around 249 K in the immersion freezing mode and at around 245 K for deposition mode nucleation. This finding agrees with a study by *Hill et al.* [2016] which also observed that heat stable ice-nucleating entities dominated the ice nucleation properties of five soil samples at temperatures below 261 K. Unfortunately, we did not have enough sample material to also investigate the effect of heat treatment at higher ambient temperatures where one might expect a larger contribution of biological material to the overall ice nucleation efficiency of soil dust samples. Also, we did not look at the impact of exposure to higher temperatures compared to this study, e.g., heating up to 573 K which was investigated by *Tobo et al.* [2014]. At temperatures above ~373 K, it is expected that not only proteinaceous structures will be destroyed but also other soil organic components will be affected.

Garcia et al. [2012] collected airborne particles over agricultural areas and subjected these samples to a heat treatment at 371 K for 20 min to denature proteins and organics. For a temperature range between 251 and 265 K, *Garcia et al.* [2012] observed a reduction of the ice nucleation efficiencies between a factor of 2 for atmospheric ice nuclei over grassland and more than 2 orders of magnitude for ice nuclei from nonirrigated crop fields. Note, however, that the exact composition of these atmospheric samples is not known even though it can be assumed that there is a large contribution by soil dust particles [*Garcia et al.*, 2012]. *Conen et al.* [2011] also observed a reduction of the ice nucleation efficiency after heating soil dust samples to a temperature of 373 K for a duration of 10 min. The ice nucleation efficiency was reduced by up to 2 orders of magnitude over a temperature range between 258 and 264 K. However, this reduction largely depended on the soil dust type. *O'Sullivan et al.* [2014] also observed a reduction of the ice nucleation efficiency after heating soil dust samples to 363 K for 10 min. The reduction of the INAS density values varied between different soil dust types. Heat treatment did not affect the ice nucleation efficiency at temperatures below 245 K. *Tobo et al.* [2014] found a reduction of the ice nucleation efficiency by applying treatments with heat (573 K) or H₂O₂. In contrast to the study by *O'Sullivan et al.* [2014], treated dusts were significantly less ice active down to temperatures around 237 K [*Tobo et al.*, 2014]. *O'Sullivan et al.* [2015] put forward initial evidence for proteinaceous (i.e., heat sensitive) ice nucleation entities being mostly associated with soil dust particles larger than 2 μm.

The comparison with the studies described above suggests that for Argentinian Soil ice nucleation efficiency at lower temperature is not primarily influenced by ice nucleation active protein structures. The role of SOM for the ice nucleation properties of agricultural soil dusts is not fully clear, and especially at higher temperatures, further investigation is needed.

Concerning the interpretation of our experimental results for lower temperatures, it should be noted that some SOM components relevant for ice nucleation caused by agricultural soil dusts may be resistant to physical treatments (e.g., heat treatment). For example, organic macromolecules such as polysaccharides are under consideration for causing the high ice nucleation activity of organic compounds at the surface of pollen particles [*Pummer et al.*, 2012]. Sugar molecules are also known to be involved in the aggregation of larger protein clusters which constitute ice nucleation active sites on bacteria [*Szyrmer and Zawadzki*, 1997].

5. Summary and Conclusions

The goal of this study was to investigate the ice nucleation properties of four soil dust samples and to establish relations between the different soil dust components and the observed INAS density values.

Three soil dust samples from agricultural areas were analyzed with regard to their SOM properties, resulting in very distinct differences. The mass fraction of total SOC varied between 1 and 3% among MS (origin: grassland), AS, and GS (origin: arable land). The sample from Mongolia contained more microorganisms (fungi and bacteria) than the samples from Northern Germany and Argentina.

The ice nucleation properties of four soil dust samples from agricultural areas were investigated in the temperature range between 233 and 262 K. The ice nucleation efficiencies were expressed by the aerosol surface area-related INAS density for all samples. The ice nucleation efficiencies were summarized by common INAS density functions despite their different physicochemical and microbiological characteristics.

The INAS densities can be described by a temperature-dependent exponential function with

$$n_s(T) = \exp(110.266 - 0.350 \cdot T) \text{ [m}^{-2}\text{]} \quad (5)$$

parameterizing immersion freezing occurring between 247 and 262 K.

For deposition nucleation, the INAS densities are expressed as an exponential function of the composite variable $x_{\text{therm}}(T, S_i)$ with

$$n_s(x_{\text{therm}}) = 5.224 \cdot 10^7 \cdot \exp(0.148 \cdot x_{\text{therm}}) \text{ [m}^{-2}\text{]} \quad (6)$$

which is a relation only valid at subsaturated conditions with respect to water and for temperatures between 233 and 246 K. The variable $x_{\text{therm}}(T, S_i)$ depends on temperature T and saturation over ice S_i . The wind-blown AS sample activated at a similar humidity than the sample derived from the top soil.

All investigated soil dusts were at least slightly more ice active than desert dusts, both in the immersion freezing and the deposition nucleation mode. Note, however, that the variability in ice nucleation properties is high for agricultural soil dusts. This variability is most likely linked to the complexity of SOM and eventually also differences in the mineral composition. In our study, primary biological particles did not seem to be the sole explanation of enhanced ice nucleation of soil dusts at temperatures around 250 K. Further experiments in particular at higher temperatures are needed to further evaluate and quantify the effect of heat treatment on the ice nucleation efficiency of several different agricultural soil dust types. The overall relevance of OM (e.g., organic coatings and organo-mineral complexes) and biological material for the ice nucleation efficiency of soil dust particles remained unclear.

Since the contributions of agricultural areas to the global dust burden may be as high as 25% [Ginoux et al., 2012], soil dust particles can be transported to upper layers of the troposphere where they are able to act as ice nuclei. The INAS density relations presented in this work can be used as a starting point to estimate the contribution of soil dust particles to atmospheric ice nuclei concentrations. The INAS density parameterization for soil dusts presented in this study can be further improved and extended by measuring the ice nucleation properties of a larger variety of soil dusts over a wider temperature range. This also means to include effects such as seasonal variations of the ice nucleation properties due to changes in the composition of SOM.

Acknowledgments

Support by the AIDA technician team is gratefully acknowledged. This research was partly funded by DFG through FOR 1525 INUIT and the Helmholtz Association through the President's Initiative and Networking Fund and the Research Program "Atmosphere and Climate (ATMO)." For the FTIR measurements, we thank Sophie Godow for the laboratory work and the German Research Foundation (DFG) for financial support (grant EL 191/7-1). The data presented in this paper can be made available upon request—please contact Ottmar Möhler (ottmar.moehler@kit.edu).

References

- Becker, R., B. Bubner, R. Remus, S. Wirth, and A. Ulrich (2014), Impact of multi-resistant transgenic Bt maize on straw decomposition and the involved microbial communities, *Appl. Soil Ecol.*, *73*, 9–18, doi:10.1016/j.apsoil.2013.08.002.
- Boucher, O., et al. (2013), Clouds and aerosols, in *IPCC Fifth Assessment Report 2013: The Physical Science Basis. Contribution of Working Group I to the Fifth Assessment Report of the Intergovernmental Panel on Climate Change*, edited by T. F. Stocker et al., pp. 571–657, Cambridge Univ. Press, Cambridge, U. K.
- Broadley, S. L., B. J. Murray, R. J. Herbert, J. D. Atkinson, S. Dobbie, T. L. Malkin, E. Condliffe, and L. Neve (2012), Immersion mode heterogeneous ice nucleation by an illite rich powder representative of atmospheric mineral dust, *Atmos. Chem. Phys.*, *12*(1), 287–307, doi:10.5194/acp-12-287-2012.
- Cahill, J. F., K. Suski, J. H. Seinfeld, R. A. Zaveri, and K. A. Prather (2012), The mixing state of carbonaceous aerosol particles in northern and southern California measured during CARES and CalNex 2010, *Atmos. Chem. Phys.*, *12*(22), 10,989–11,002, doi:10.5194/acp-12-10989-2012.
- Capriel, P., T. Beck, H. Borchert, J. Gronholz, and G. Zachmann (1995), Hydrophobicity of the organic matter in arable soils, *Soil Biol. Biochem.*, *27*(11), 1453–1458, doi:10.1016/0038-0717(95)00068-P.
- Celi, L., M. Schnitzer, and M. Nègre (1997), Analysis of carboxyl groups in soil humic acids by a wet chemical method, fourier-transform infrared spectrophotometry, and solution-state carbon-13 nuclear magnetic resonance: A comparative study, *Soil Sci.*, *162*(3), 189–197, doi:10.1097/00010694-199703000-00004.
- Christner, B. C., C. E. Morris, C. M. Foreman, R. Cai, and D. C. Sands (2008), Ubiquity of biological ice nucleators in snowfall, *Science*, *319*(5867), 1214, doi:10.1126/science.1149757.
- Conen, F., C. E. Morris, J. Leifeld, M. V. Yakutin, and C. Alewell (2011), Biological residues define the ice nucleation properties of soil dust, *Atmos. Chem. Phys.*, *11*(18), 9643–9648, doi:10.5194/acp-11-9643-2011.
- Conen, F., E. Stopelli, and L. Zimmermann (2016), Clues that decaying leaves enrich Arctic air with ice nucleating particles, *Atmos. Environ.*, *129*, 91–94, doi:10.1016/j.atmosenv.2016.01.027.
- Connolly, P. J., O. Möhler, P. R. Field, H. Saathoff, R. Burgess, T. Choularton, and M. Gallagher (2009), Studies of heterogeneous freezing by three different desert dust samples, *Atmos. Chem. Phys.*, *9*(8), 2805–2824, doi:10.5194/acp-9-2805-2009.
- Creamean, J. M., et al. (2013), Dust and biological aerosols from the Sahara and Asia influence precipitation in the Western U.S., *Science*, *339*(6127), 1572–1578, doi:10.1126/science.1227279.
- Cziczo, D. J., K. D. Froyd, C. Hoose, E. J. Jensen, M. Diao, M. A. Zondlo, J. B. Smith, C. H. Twohy, and D. M. Murphy (2013), Clarifying the dominant sources and mechanisms of cirrus cloud formation, *Science*, *340*(6138), 1320–1324, doi:10.1126/science.1234145.
- DeMott, P. J., D. J. Cziczo, A. J. Prenni, D. M. Murphy, S. M. Kreidenweis, D. S. Thomson, R. Borys, and D. C. Rogers (2003), Measurements of the concentration and composition of nuclei for cirrus formation, *Proc. Natl. Acad. Sci. U.S.A.*, *100*(25), 14,655–14,660, doi:10.1073/pnas.2532677100.

- DeMott, P. J., A. J. Prenni, X. Liu, S. M. Kreidenweis, M. D. Petters, C. H. Twohy, M. S. Richardson, T. Eidhammer, and D. C. Rogers (2010), Predicting global atmospheric ice nuclei distributions and their impacts on climate, *Proc. Natl. Acad. Sci. U.S.A.*, *107*(25), 11,217–11,222, doi:10.1073/pnas.0910818107.
- Després, V. R., et al. (2012), Primary biological aerosol particles in the atmosphere: A review, *Tellus, Ser. B*, *64*, 15,598, doi:10.3402/tellusb.v64i0.15598.
- Ellerbrock, R. H., H. H. Gerke, J. Bachmann, and M.-O. Goebel (2005), Composition of organic matter fractions for explaining wettability of three forest soils, *Soil Sci. Soc. Am. J.*, *69*(1), 57–66, doi:10.2136/sssaj2005.0057.
- Fahey, D. W., et al. (2014), The AquaVIT-1 intercomparison of atmospheric water vapor measurement techniques, *Atmos. Meas. Tech.*, *7*, 3177–3213, doi:10.5194/amt-7-3177-2014.
- Fierer, N., J. A. Jackson, R. Vilgalys, and R. B. Jackson (2005), Assessment of soil microbial community structure by use of taxon-specific quantitative PCR assays, *Appl. Environ. Microbiol.*, *71*(7), 4117–4120, doi:10.1128/AEM.71.7.4117-4120.20.
- Foot, V. E., P. H. Kaye, W. R. Stanley, S. J. Barrington, M. Gallagher, and A. Gabey (2008), Low-cost real-time multiparameter bio-aerosol sensors, *Proc. SPIE*, *7116*, doi:10.1117/12.800226.
- Fornea, A. P., S. D. Brooks, J. B. Dooley, and A. Saha (2009), Heterogeneous freezing of ice on atmospheric aerosols containing ash, soot, and soil, *J. Geophys. Res.*, *114*, D13201, doi:10.1029/2009JD011958.
- Forster, P., et al. (2007), Changes in atmospheric constituents and in radiative forcing, in *Climate Change: The Physical Science Basis. Contribution of Working Group I to the Fourth Assessment Report of the Intergovernmental Panel on Climate Change*, edited by S. Solomon et al., pp. 131–234, Cambridge Univ. Press, Cambridge, U. K.
- Funk, R., and H. I. Reuter (2006), Wind erosion, in *Soil Erosion in Europe*, edited by J. Boardman and J. Poesen, pp. 563–582, John Wiley, Chichester, U. K., doi:10.1002/0470859202.
- Funk, R., E. Skidmore, and L. Hagen (2004), Comparison of wind erosion measurements in Germany with simulated soil losses by WEPS, *Environ. Modell. Software*, *19*, 177–183, doi:10.1016/S1364-8152(03)00120-8.
- Gaiero, D. M., P. J. Depetris, J. L. Probst, S. M. Bidart, and L. Leleyter (2004), The signature of river- and wind-borne materials exported from Patagonia to the southern latitudes: A view from REEs and implications for paleoclimatic interpretations, *Earth Planet. Sci. Lett.*, *219*, 357–376, doi:10.1016/S0012-821X(03)00686-1.
- Gallavardin, S., U. Lohmann, and D. Cziczo (2008), Analysis and differentiation of mineral dust by single particle laser mass spectrometry, *Int. J. Mass Spectrom.*, *274*(1–3), 56–63, doi:10.1016/j.jjms.2008.04.031.
- Garcia, E., T. C. J. Hill, A. J. Prenni, P. J. DeMott, G. D. Franc, and S. M. Kreidenweis (2012), Biogenic ice nuclei in boundary layer air over two U.S. High Plains agricultural regions, *J. Geophys. Res.*, *117*, D18209, doi:10.1029/2012JD018343.
- Gard, E., J. E. Mayer, B. D. Morrical, T. Dienes, D. P. Ferguson, and K. A. Prather (1997), Real-time analysis of individual atmospheric aerosol particles: Design and performance of a portable ATOFMS, *Anal. Chem.*, *69*(20), 4083–4091, doi:10.1021/ac970540n.
- Ginoux, P., J. M. Prospero, T. E. Gill, N. C. Hsu, and M. Zhao (2012), Global-scale attribution of anthropogenic and natural dust sources and their emission rates based on MODIS Deep Blue aerosol products, *Rev. Geophys.*, *50*, RG3005, doi:10.1029/2012RG000388.
- Gottwald, W., and G. Wachter (1997), *IR-Spektroskopie für Anwender*, Wiley-VCH, Weinheim, Germany.
- Hallar, A. G., G. Chirokova, I. McCubbin, T. H. Painter, C. Wiedinmyer, and C. Dodson (2011), Atmospheric bioaerosols transported via dust storms in the western United States, *Geophys. Res. Lett.*, *38*, L17801, doi:10.1029/2011GL048166.
- Hill, T. C. J., P. J. DeMott, Y. Tobo, J. Fröhlich-Nowoisky, B. F. Moffett, G. D. Franc, and S. M. Kreidenweis (2016), Sources of organic ice nucleating particles in soils, *Atmos. Chem. Phys.*, *16*, 7195–7211, doi:10.5194/acp-16-7195-2016.
- Hiranuma, N., et al. (2015), A comprehensive laboratory study on the immersion freezing behavior of illite NX particles: A comparison of 17 ice nucleation measurement techniques, *Atmos. Chem. Phys.*, *15*, 2489–2518, doi:10.5194/acp-15-2489-2015.
- Hoose, C., and O. Möhler (2012), Heterogeneous ice nucleation on atmospheric aerosols: A review of results from laboratory experiments, *Atmos. Chem. Phys.*, *12*(20), 9817–9854, doi:10.5194/acp-12-9817-2012.
- Isono, K., and Y. Ikebe (1960), On the ice-nucleating ability of rock-forming minerals and soil particles, *J. Meteorol. Soc. Jpn.*, *38*(5), 213–230.
- Kaye, P. H., W. R. Stanley, E. Hirst, E. V. Foot, K. L. Baxter, and S. J. Barrington (2005), Single particle multichannel bio-aerosol fluorescence sensor, *Opt. Express*, *13*(10), 3583–3593, doi:10.1364/OPEX.13.003583.
- Kögel-Knabner, I., G. Guggenberger, M. Kleber, E. Kandeler, K. Kalbitz, S. Scheu, K. Eusterhues, and P. Leinweber (2008), Organo-mineral associations in temperate soils: Integrating biology, mineralogy, and organic matter chemistry, *J. Plant Nutr. Soil Sci.*, *171*(1), 61–82, doi:10.1002/jpln.200700048.
- MacCarthy, P., and J. A. Rice (1985), Spectroscopic methods (other than NMR) for determining functions in humic substances, in *Humic Substances in Soil, Sediment, and Water: Geochemistry, Isolation and Characterization*, edited by G. R. Aiken et al., Wiley Interscience, New York.
- Madejova, J., and P. Komadel (2001), Baseline studies of the Clay Minerals Society source clays: Infrared methods, *Clays Clay Miner.*, *49*(5), 410–432, doi:10.1346/CCMN.2001.0490508.
- Marcolli, C. (2014), Deposition nucleation viewed as homogeneous or immersion freezing in pores and cavities, *Atmos. Chem. Phys.*, *14*, 2071–2104, doi:10.5194/acp-14-2071-2014.
- Möhler, O., et al. (2006), Efficiency of the deposition mode ice nucleation on mineral dust particles, *Atmos. Chem. Phys.*, *6*(10), 3007–3021, doi:10.5194/acp-6-3007-2006.
- Möhler, O., S. Benz, H. Saathoff, M. Schnaiter, R. Wagner, J. Schneider, S. Walter, V. Ebert, and S. Wagner (2008), The effect of organic coating on the heterogeneous ice nucleation efficiency of mineral dust aerosols, *Environ. Res. Lett.*, *3*, 025007, doi:10.1088/1748-9326/3/2/025007.
- Morrison, R. T., and R. N. Boyd (1986), *Lehrbuch der Organischen Chemie*, 3rd ed., Wiley-VCH, Weinheim, Germany.
- Murphy, D. M., and T. Koop (2005), Review of the vapour pressures of ice and supercooled water for atmospheric applications, *Q. J. R. Meteorol. Soc.*, *131*(608), 1539–1565, doi:10.1256/qj.04.94.
- Murray, B. J., D. O'Sullivan, J. D. Atkinson, and M. E. Webb (2012), Ice nucleation by particles immersed in supercooled cloud droplets, *Chem. Soc. Rev.*, *41*(19), 6519–6554, doi:10.1039/c2cs35200a.
- Niemand, M., et al. (2012), A particle-surface-area-based parameterization of immersion freezing on desert dust particles, *J. Atmos. Sci.*, *69*(10), 3077–3092, doi:10.1175/JAS-D-11-0249.1.
- O'Sullivan, D., B. J. Murray, T. L. Malkin, T. F. Whale, N. S. Umo, J. D. Atkinson, H. C. Price, K. J. Baustian, J. Browse, and M. E. Webb (2014), Ice nucleation by fertile soil dusts: Relative importance of mineral and biogenic components, *Atmos. Chem. Phys.*, *14*(4), 1853–1867, doi:10.5194/acp-14-1853-2014.
- O'Sullivan, D., B. J. Murray, J. F. Ross, T. F. Whale, H. C. Price, J. D. Atkinson, N. S. Umo, and M. E. Webb (2015), The relevance of nanoscale biological fragments for ice nucleation in clouds, *Sci. Rep.*, *5*, 8082, doi:10.1038/srep08082.

- O'Sullivan, D., B. J. Murray, J. F. Ross, and M. E. Webb (2016), The adsorption of fungal ice-nucleating proteins on mineral dusts: A terrestrial reservoir of atmospheric ice-nucleating particles, *Atmos. Chem. Phys.*, *16*, 7879–7887, doi:10.5194/acp-16-7879-2016.
- Pöhlker, C., J. A. Huffman, and U. Pöschl (2011), Autofluorescence of atmospheric bioaerosols—Fluorescent biomolecules and potential interferences, *Atmos. Meas. Tech.*, *5*(1), 37–71, doi:10.5194/amt-5-37-2012.
- Pratt, K. A., and K. A. Prather (2010), Aircraft measurements of vertical profiles of aerosol mixing states, *J. Geophys. Res.*, *115*, D11305, doi:10.1029/2009JD013150.
- Pratt, K. A., P. J. DeMott, J. R. French, Z. Wang, D. L. Westphal, A. J. Heymsfield, C. H. Twohy, A. J. Prenni, and K. A. Prather (2009), In situ detection of biological particles in cloud ice-crystals, *Nat. Geosci.*, *2*, 398–401, doi:10.1038/ngeo521.
- Prenni, A. J., M. D. Petters, S. M. Kreidenweis, C. L. Heald, S. T. Martin, P. Artaxo, R. M. Garland, A. G. Wollny, and U. Pöschl (2009), Relative roles of biogenic emissions and Saharan dust as ice nuclei in the Amazon basin, *Nat. Geosci.*, *2*, 402–405, doi:10.1038/ngeo517.
- Pruppacher, H. R., and J. D. Klett (1997), *Microphysics of Clouds and Precipitation*, 2nd rev. and enl. ed., Kluwer, Dordrecht, Netherlands.
- Pummer, B. G., H. Bauer, J. Bernardi, S. Bleicher, and H. Grothe (2012), Suspendable macromolecules are responsible for ice nucleation activity of birch and conifer pollen, *Atmos. Chem. Phys.*, *12*(5), 2541–2550, doi:10.5194/acp-12-2541-2012.
- Schnell, R. C., and G. Vali (1972), Atmospheric ice nuclei from decomposing vegetation, *Nature*, *236*(5343), 163–165, doi:10.1038/236163a0.
- Shinoda, M., J. A. Gillies, M. Mikami, and Y. Shao (2011), Temperate grasslands as a dust source: Knowledge, uncertainties and challenges, *Aeolian Res.*, *3*, 271–293, doi:10.1016/j.aeolia.2011.07.001.
- Steinke, I., C. Hoose, O. Möhler, P. Connolly, and T. Leisner (2015), A new temperature and humidity dependent surface site density approach for deposition ice nucleation, *Atmos. Chem. Phys.*, *15*, 3703–3717, doi:10.5194/acp-15-3703-2015.
- Szyrmer, W., and I. Zawadzki (1997), Biogenic and anthropogenic sources of ice-forming nuclei: A review, *Bull. Am. Meteorol. Soc.*, *78*(2), 209–228, doi:10.1175/1520-0477(1997)078<0209:baasoi>2.0.co;2.
- Tegen, I., and I. Y. Fung (1995), Contribution to the mineral aerosol load from land surface modification, *J. Geophys. Res.*, *100*, 18,707–18,726, doi:10.1029/95JD02051.
- Tegen, I., M. Werner, S. P. Harrison, and K. E. Kohfeld (2004), Relative importance of climate and land use in determining present and future global soil dust emission, *Geophys. Res. Lett.*, *31*, L05105, doi:10.1029/2003GL019216.
- Tobo, Y., P. J. DeMott, T. C. J. Hill, A. J. Prenni, N. G. Swoboda-Colberg, G. D. Franc, and S. M. Kreidenweis (2014), Organic matter matters for ice nuclei of agricultural soil origin, *Atmos. Chem. Phys.*, *14*, 8521–8531, doi:10.5194/acp-14-8521-2014.
- Toprak, E., and M. Schnaiter (2013), Fluorescent biological aerosol particles measured with the Waveband Integrated Bioaerosol Sensor WIBS-4: Laboratory tests combined with a one year field study, *Atmos. Chem. Phys.*, *13*(1), 225–243, doi:10.5194/acp-13-225-2013.
- Vali, G. (2008), Repeatability and randomness in heterogeneous freezing nucleation, *Atmos. Chem. Phys.*, *8*(16), 5017–5031, doi:10.5194/acp-8-5017-2008.
- Vali, G., P. J. DeMott, O. Möhler, and T. F. Whale (2015), Technical note: A proposal for ice nucleation terminology, *Atmos. Chem. Phys.*, *15*, 10,263–10,270, doi:10.5194/acp-15-10263-2015.
- Van der Marel, H. W., and H. Beutelspacher (1976), *Atlas of Infrared Spectroscopy of Clay Minerals and Their Admixtures*, Elsevier, Amsterdam.
- Wagner, R., and O. Möhler (2013), Heterogeneous ice nucleation ability of crystalline sodium chloride dihydrate particles, *J. Geophys. Res. Atmos.*, *118*, 4610–4622, doi:10.1002/jgrd.50325.
- Willerslev, E., A. J. Hansen, R. Rønn, T. B. Brand, I. Barnes, C. Wiuf, D. Gilichinsky, D. Mitchell, and A. Cooper (2004), Long-term persistence of bacterial DNA, *Curr. Biol.*, *14*(1), R9–R10, doi:10.1016/j.cub.2003.12.012.
- Yan, H., S. Wang, C. Wang, G. Zhang, and N. Patels (2005), Losses of soil organic carbon under wind erosion in China, *Global Change Biol.*, *11*, 828–840, doi:10.1111/j.1365-2486.2005.00950.x.